ACCOUNTS of chemical research

Article

pubs.acs.org/accounts

Oxygen Transport in Perovskite-Type Solid Oxide Fuel Cell Materials: Insights from Quantum Mechanics

Ana B. Muñoz-García,[†] Andrew M. Ritzmann,[‡] Michele Pavone,[†] John A. Keith,[§] and Emily A. Carter*[,∥]

[†]Department of Chemical Sciences, University of Naples Federico II, Naples 80126, Italy

[‡]Department of Chemical and Biological Engineering, Princeton University, Princeton, New Jersey 08544-5263, United States

[§]Department of Chemical and Petroleum Engineering, University of Pittsburgh, Pittsburgh, Pennsylvania 15261, United States

[∥]Deparment of Mechanical and Aerospace Engineering, Program in Applied and Computational Mathematics, and Andlinger Center for Energy and the Environment, Princeton University, Princeton, New Jersey 08544-5263, United States

CONSPECTUS: Global advances in industrialization are precipitating increasingly rapid consumption of fossil fuel resources and heightened levels of atmospheric CO_2. World sustainability requires viable sources of renewable energy and its efficient use. First-principles quantum mechanics (QM) studies can help guide developments in energy technologies by characterizing complex material properties and predicting reaction mechanisms at the atomic scale. QM can provide unbiased, qualitative guidelines for experimentally tailoring materials for energy applications.

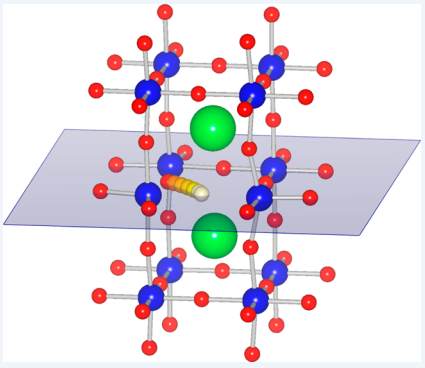

This Account primarily reviews our recent QM studies of electrode materials for solid oxide fuel cells (SOFCs), a promising technology for clean, efficient power generation. SOFCs presently must operate at very high temperatures to allow transport of oxygen ions and electrons through solid-state electrolytes and electrodes. High temperatures, however, engender slow startup times and accelerate material degradation. SOFC technologies need cathode and anode materials that function well at lower temperatures, which have been realized with mixed ion−electron conductor (MIEC) materials.

Unfortunately, the complexity of MIECs has inhibited the rational tailoring of improved SOFC materials. Here, we gather theoretically obtained insights into oxygen ion conductivity in two classes of perovskite-type materials for SOFC applications: the conventional $La_{1-x}Sr_xMO_3$ family (M = Cr, Mn, Fe, Co) and the new, promising class of $Sr_2Fe_{2-x}Mo_xO_6$ materials. Using density functional theory + U (DFT+U) with $U-J$ values obtained from *ab initio* theory, we have characterized the accompanying electronic structures for the two processes that govern ionic diffusion in these materials: (i) oxygen vacancy formation and (ii) vacancy-mediated oxygen migration. We show how the corresponding macroscopic oxygen diffusion coefficient can be accurately obtained in terms of microscopic quantities calculated with first-principles QM.

We find that the oxygen vacancy formation energy is a robust descriptor for evaluating oxide ion transport properties. We also find it has a direct relationship with (i) the transition metal−oxygen bond strength and (ii) the extent to which electrons left behind by the departing oxygen delocalize onto the oxygen sublattice. Design principles from our QM results may guide further development of perovskite-based MIEC materials for SOFC applications.

1. INTRODUCTION

Fossil-fuel-driven industrialization hastens a daunting two-sided problem: nonrenewable natural resources are depleted while atmospheric CO_2 concentrations alarmingly increase. Efficient, renewable, and CO_2-neutral energy technologies are needed. Solid oxide fuel cells (SOFCs) can potentially deliver clean and highly efficient power via electrochemistry. SOFC electrolytes, anodes, and cathodes can be manufactured from low-cost ceramic materials. However, cathode and anode materials carry high intrinsic activation energies for ionic conductivity. That inevitably leads to high operating temperatures (T_{op} = 800−1000 °C) that cause deleterious thermal stresses, high start-up energy inputs, and short cell lifetimes.[1] Simply reducing SOFC operation temperatures would curb oxygen diffusion and confine the oxygen reduction reaction (ORR) to occur only at the triple phase boundary between air, the cathode, and the electrolyte; therefore, lower temperatures engender higher overpotentials. Mixed ion-electron conductor (MIEC) cathode materials permit lower T_{op} by increasing the active area for ORR via facile bulk ion transport (Figure 1). MIEC cathodes therefore can provide lower overpotentials and improved ORR kinetics[2] in intermediate temperature (IT-)SOFCs ($T_{op} \approx$ 600−800 °C). Although MIEC cathode materials are promising, further improvements are needed before SOFCs would be deployed widely.

Understanding oxygen ion mobility is critical to improving MIEC materials.[3−5] Common MIECs are based on perovskite-type transition metal (TM) oxides with the stoichiometric formula AMO_3 (A = La and/or Sr; M = Mn, Fe, Co, and/or Cr). Oxygen ion transport through these lattices occurs via vacancy-mediated

Special Issue: DFT Elucidation of Materials Properties

Received: December 26, 2013
Published: June 27, 2014

   dx.doi.org/10.1021/ar4003174 | Acc. Chem. Res. 2014, 47, 3340−3348

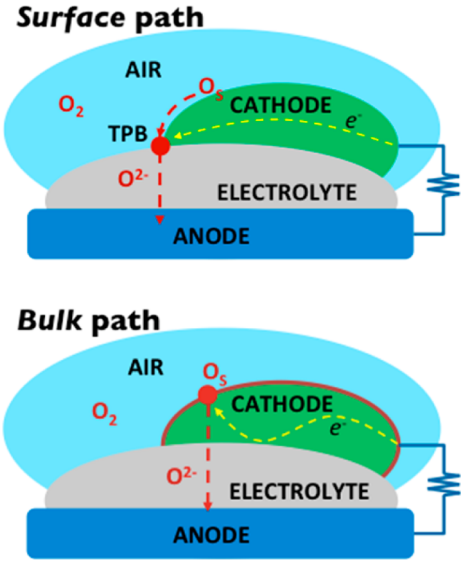

Figure 1. Two possible oxygen incorporation paths: *surface path* showing the triple-phase boundary (TPB) and *bulk path* highlighting in red the increased active area for the oxygen reduction reaction.

"hopping" mechanisms. The oxide ion diffusion coefficient, D, has an Arrhenius form: $D = A{\cdot}\exp[-Q/(k_BT)]$, where the overall activation energy Q comprises two terms: (1) the oxygen vacancy formation free energy and (2) the activation enthalpy to transport an O^{2-} to its nearest vacant site. Consequently, high bulk conductivity requires low oxygen vacancy formation energies and low migration barrier heights.

Experimental measurements can determine D for existing materials, but they usually cannot reveal design principles that improve D. Thus, materials optimization usually proceeds by trial and error, requiring expensive, time-consuming syntheses. Rational materials optimization can benefit from fundamental, atomic-scale insights that explain *how and why* structural and electronic factors affect oxygen bulk conductivity. Using theory to understand oxide ion transport in SOFCs helps direct experimentalists toward promising new materials while also creating a feedback loop to improve theory. This Account summarizes our recent computational efforts to provide these insights.

Some oxides (including the perovskites discussed herein) are strongly correlated materials, since highly localized electrons at the TM sites govern their material properties. Standard Kohn–Sham density functional theory[6] (KS-DFT) often fails to accurately predict physical properties of these materials. We outline procedures to overcome these failures. We then summarize insights from explicitly modeling oxygen vacancy formation and oxide ion diffusion in two classes of materials: the conventional Sr-doped $LaMO_3$ (M = Cr, Mn, Fe, Co) perovskites and the new, promising $Sr_2Fe_{2-x}Mo_xO_6$ materials. The first class represents the state-of-the-art for both applications in high-temperature SOFCs and MIEC-based IT-SOFCs.[7] The second class with $x = 0.5$, $Sr_2Fe_{1.5}Mo_{0.5}O_6$ ($SFMO_{0.5}$), has recently demonstrated outstanding electrocatalytic performance in symmetric SOFCs.[8] We conclude by rationalizing experimentally observed material properties through their electronic, magnetic, and structural features, showing how quantum mechanics (QM) may help guide next-generation IT-SOFC development.

2. DFT+U FOR PHYSICALLY CORRECT DESCRIPTIONS OF STRONGLY CORRELATED MATERIALS

KS-DFT is widely used in first-principles QM studies of extended materials because of its relative accuracy and computational efficiency. Exchange-correlation (XC) functionals utilizing local (LDA) and semilocal (GGA) approximations often sufficiently predict many different material properties. However, the inexact exchange energy approximation in these XC functionals introduces self-interaction errors (SIEs) that can result in overly delocalized electron densities and other unphysical behaviors. SIEs become most significant when multiple open-shell electrons reside within tightly contracted orbitals, such as in d or f electrons in some TM oxides.[9]

Out of several SIE correcting approaches,[10] two are summarized here. DFT+U theory applies an averaged intra-atomic electron–electron potential to the electrons in the subset of atomic orbitals that are highly susceptible to SIE, providing a more physically correct description of Coulomb (U) and exchange (J) interactions within this subset.[11] This computationally efficient treatment uses a single $U-J$ parameter, but deriving this parameter from *ad hoc* experimental data introduces empiricism that impairs transferability for other predictions. Obtaining this parameter from first-principles theory is possible but not trivial. Alternatively, hybrid DFT adds to all electrons (rather than just a subset) a partial amount of exact, nonlocal exchange energy from Hartree–Fock theory to offset the SIE.[12] While accounting for SIEs from all electrons, hybrid DFT solved with plane-wave basis sets and periodic boundary conditions is computationally expensive due to the nonlocal exchange integral evaluations in real space. Since DFT+U and hybrid DFT often provide qualitatively similar results, we employ DFT+U whenever it has been confirmed to describe the correct physics of the material. We wish to predict properties of materials with oxygen vacancies, so we use the GGA functional of Perdew, Burke, and Ernzerhof (PBE),[13] which better describes bond energies and reaction energetics (such as the loss of O_2) than LDA.[14]

We derive $U-J$ parameters using the *ab initio* scheme of Mosey, Liao, and Carter.[15,16] Here, a unique $U-J$ value for each TM element is obtained from unrestricted Hartree–Fock (UHF) calculations on electrostatically embedded clusters. This unbiased approach requires no experimental data apart from crystal and magnetic structures, allowing DFT+U calculations to be maximally independent of experiment with transferability in predictions. We furthermore contend that this approach is closer to the physical meaning of the U and J parameters than first-principles approaches that derive these from DFT calculations using linear-response theory.[17] We previously showed that this *ab initio* DFT+U scheme succeeds for iron, chromium, nickel, and manganese oxides,[16,18,19] materials that standard DFT describes poorly. Very recently, a comparison of the linear-response versus UHF approaches revealed serious limitations for the former but not the latter.[20]

Indeed, conventional DFT also incorrectly predicts electronic and magnetic features of $LaMO_3$ perovskites. For example, LDA and GGA predict $LaMnO_3$ to have a ferromagnetic metallic ground state, while in reality it is an antiferromagnetic (AFM) insulator.[21] Instead, properties from *ab initio*-derived DFT+U theory of $LaFeO_3$, $LaCoO_3$, and Sr-doped $LaMO_3$ qualitatively agree with measurements. Likewise, the SIE in PBE causes an incorrect description of the parent material $Sr_2Fe_{2-x}Mo_xO_6$ with $x = 1$ ($SFMO_{1.0}$), which is predicted to be

dx.doi.org/10.1021/ar4003174 | Acc. Chem. Res. 2014, 47, 3340–3348

a nonmagnetic semiconductor. By contrast, the experimentally observed half-metallic AFM character of $SFMO_{1.0}$[22] is correctly described by PBE+U (Figure 2).

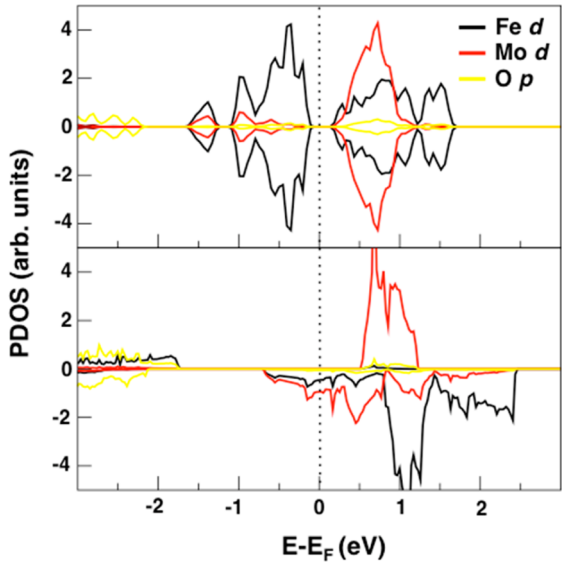

Figure 2. Projected densities of states (PDOS) on Fe d, Mo d, and O p orbitals of $SFMO_{1.0}$ predicted by PBE (top panel) and PBE+U (bottom panel). Positive/negative PDOS refer to α-/β-spin electrons. Fermi energies set to be zero. Adapted from ref 26.

3. OXYGEN VACANCY FORMATION ENERGY

Oxygen vacancy formation can be expressed according to eq 1 (in Kröger–Vink notation):[23]

$$2M_M^X + O_O^X \rightarrow 2M_M' + V_O^{\bullet\bullet} + \frac{1}{2}O_2(g) \quad (1)$$

The reaction enthalpy can be obtained by calculating energies for the perfect lattice (with an oxygen O_O^x between two TM ions M_M^x), the defective lattice with an oxygen vacancy ($V_O^{\bullet\bullet}$) and its two adjacent reduced metal sites (M_M'), and the oxygen molecule in gas phase in its triplet ground state.

Creating a $V_O^{\bullet\bullet}$ by removing a neutral oxygen atom leads to defective $AMO_{3-\delta}/Sr_2Fe_{2-x}Mo_xO_{6-\delta}$ lattices, with a non-stoichiometry degree (δ) that depends on the periodic supercell model size. We obtain the electronic energies and crystal vibrations of structurally relaxed perfect/defective structures ($E_{perfect}/E_{defective}$) from spin-polarized DFT+U calculations using the Vienna Ab Initio Simulation Package (VASP).[24] Further computational details (structural models, convergence parameters, U–J values, magnetic arrangements of M sublattices) can be found elsewhere.[25−32] The simplest approximation of the vacancy formation free energy for eq 1 can be directly obtained from electronic energies (eq 2):

$$\Delta E_{f,vac} = E_{defective} - E_{perfect} + \frac{1}{2}E_{O_2} \quad (2)$$

We previously showed that additional zero-point and thermal energy contributions affect the reaction enthalpy by less than 0.1 eV in LSF (x_{Sr} = 0, 0.25, 0.50).[29] Thus, we use $\Delta E_{f,vac}$ to analyze trends for perovskite materials.

3.1. $LaMO_3$

Calculated values for $\Delta E_{f,vac}$ for $LaMO_3$ (M = Cr, Mn, Fe, Co) are shown in Figure 3 (top). PBE+U $\Delta E_{f,vac}$ values are largely

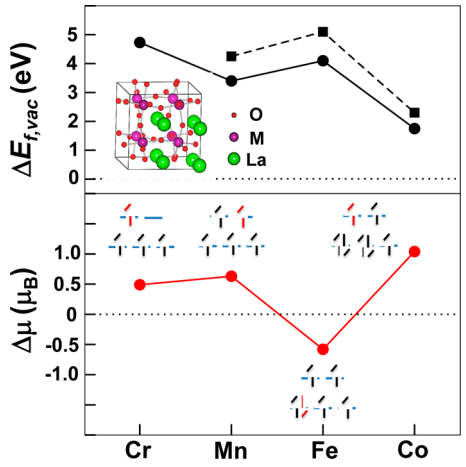

Figure 3. (top) Oxygen vacancy formation energies, $\Delta E_{f,vac}$, for $LaMO_3$ (M = Cr, Mn, Fe, Co). PBE+U (solid line) and experimental (dashed line) values are shown. Adapted from ref 25. (bottom) Magnetic moment variations of the nearby M ion upon formation of an oxygen vacancy. Schematic of the d orbital occupation of M ions before (M^{3+}, black half-arrows) and after (M^{2+}, extra red half-arrow representing the electron added upon reduction) formation of an oxygen vacancy.

consistent with experimental data from thermogravimetric analyses. Calculated $\Delta E_{f,vac}$ values do not monotonically decrease with increasing atomic number. This trend matches experimental bulk oxide ion diffusion rates for these four materials as well.[33] Notably, the consistent errors between theory and experiment are approximately halved when accounting for the error associated with the known overbinding of O_2 by DFT-GGA.

With QM calculations, we can elucidate the origins of this trend by analyzing how the electronic structure changes upon $V_O^{\bullet\bullet}$ formation.[25] After removal of a neutral oxygen atom from the ideal lattice by breaking two TM–O bonds, the two electrons formerly associated with the formally O^{2-} ion must redistribute within the defective crystal. Figure 4 shows electron density difference plots illustrating how this remaining charge localizes on the two TMs closest to the vacancy. This localized reduction is consistent with a decrease of atomic Bader charge[34] (by ~0.4e) of each TM nearest the vacancy. Bader charges of La remain unaltered, so La ions are merely spectators during this process. The thermodynamics of $V_O^{\bullet\bullet}$ formation therefore depend on M–O–M bond strengths and the electron affinity of the two adjacent TM ions that reduce from M^{3+} to M^{2+}. Lower $\Delta E_{f,vac}$ values are obtained with weaker TM–O bonds and/or M^{3+} TMs with higher electron affinities. Regarding TM–O bond strengths, early TMs having low d occupation form strong polar–covalent, donor–acceptor bonds with oxygen whereas late TMs with doubly occupied d orbitals create repulsion with oxygen lone pairs that weaken TM–O bonds.[35] This is well-understood by inorganic chemists in terms of the heuristically observed "oxo wall".[36] To understand electron affinities of M^{3+} ions, we analyze the configuration of their d^n shells before and after oxygen vacancy formation. Measured and computed magnetic moments show that Cr^{3+} and Mn^{3+} ions are high spin (HS) whereas Co^{3+} can be considered intermediate spin (IS) at SOFC operating temperatures (*vide infra*). In these cases, the magnetic moment increases when the oxygen is removed (due to the electrons left behind entering the majority spin manifold). The increased magnetic moment brings increased

dx.doi.org/10.1021/ar4003174 | Acc. Chem. Res. 2014, 47, 3340−3348

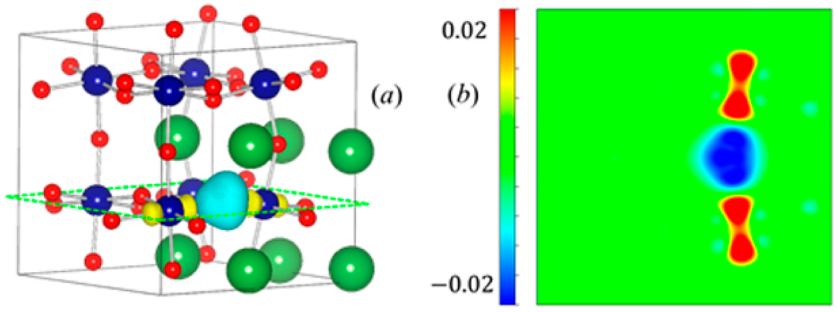

Figure 4. Electron density differences (e^-/bohr^3) upon oxygen vacancy formation in $LaCrO_3$: (a) 3D isosurface. Yellow/cyan surface refers to an accumulation/loss of electrons. (b) 2D slice along the (100) plane. Red contours (accumulated electronic density) indicate localized reduction of neighboring TM ions. Figure from ref 25. Reproduced by permission of The Royal Society of Chemistry.

favorable exchange interaction energy and causes a lower $\Delta E_{f,vac}$. By contrast, when the extra electrons are added necessarily to the minority spin manifold in Fe^{3+}, reduction produces Fe^{2+} with a decreased magnetic moment. This provides no extra favorable exchange and leads to extra Coulomb repulsion within a doubly occupied d orbital. For these reasons, the increase of magnetic moment on the TM ions correlates (inversely) with the $\Delta E_{f,vac}$ trend (Figure 3, bottom).

Such a correlation has consequences for $LaCoO_3$. Motivated by the controversy around the actual spin state of $LaCoO_3$ (invoked to be a mixture of Co^{3+} low spin (LS), IS, and HS states to explain some anomalous properties[37]), we have explicitly analyzed oxygen vacancy formation for several $LaCoO_3$ spin states: LS, IS, HS, and a 1:1 mixture of HS and LS. We find that LS Co^{3+} has the lowest $\Delta E_{f,vac}$ among the spin states surveyed, which again can be rationalized in terms of higher exchange stabilization upon reduction. The LS Co^{3+} ion (t_{2g}^6 e_g^0) gains four favorable exchange interactions upon reduction to HS Co^{2+} (t_{2g}^5 e_g^2), which offsets the added Coulomb repulsion from the additional electron, the cost of promoting an electron from the t_{2g} orbitals to the e_g orbitals, and the extra energy required to break the stronger (LS Co^{3+})−O bond.[38] We then predict that $LaCoO_3$ oxygen vacancy concentrations would be higher in materials with more LS Co^{3+}.[32]

3.2. $La_{1-x}Sr_xMO_3$

Large divalent cations (e.g., Sr^{2+}, Ca^{2+}, Ba^{2+}) can serve as A-site substitutions for La^{3+} in $LaMO_3$-based SOFC cathodes to increase charge carrier (hole) concentrations and enhance p-type conductivity. Adding Sr^{2+} induces the formation of a (formally) TM^{4+} to maintain electroneutrality. These holes affect the material valence band edge and qualitatively change the electronic structure, resulting in completely new material properties.

To understand this phenomenon, we analyzed $La_{1-x}Sr_xMnO_3$ (LSM) and $La_{1-x}Sr_xFeO_3$ (LSF) with x_{Sr} = 0.25 and 0.5. LSM is a common high-temperature SOFC cathode material, a good electro-catalyst but a poor oxide ion conductor. LSF exhibits good bulk oxide ion transport and is the base material for the prototypical MIEC cathode, $La_{0.75}Sr_{0.25}Co_{0.2}Fe_{0.8}O_3$.[39] We recently evaluated how Sr doping affects the electronic structures of these two materials.[29,31] Figure 5 (top) displays $\Delta E_{f,vac}$ versus Sr content (x_{Sr}) in both materials. $\Delta E_{f,vac}(x_{Sr})$ of LSM and LSF follow the same trend in which the presence of Sr lowers the vacancy formation energy due to favorable charge compensation (excess Sr-derived holes compensated by excess O-vacancy-derived electrons). This trend is consistent with measurements showing that Sr-doped $LaMO_3$ materials exhibit improved oxide

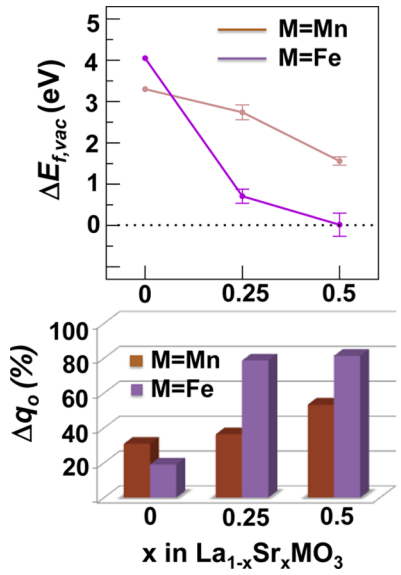

Figure 5. (top) Oxygen vacancy formation energies, $\Delta E_{f,vac}$, for $La_{1-x}Sr_xMO_3$ (M = Mn, Fe). (bottom) Percentage of electrons delocalized over the oxygen sublattice after oxygen vacancy formation.

ion bulk diffusion.[40] The effect of x_{Sr} on $\Delta E_{f,vac}$ is less for LSM than for LSF. Our electronic structure analysis does not support a rationalization based on localized reduction; a subtler picture arises, as discussed next.

As noted earlier, the nearest TM ions receive most of the extra charge in both $LaMnO_3$ and $LaFeO_3$ ($La_{1-x}Sr_xMO_3$ with x_{Sr} = 0). Only ∼30% and ∼20% of this charge goes into the oxygen sublattice for M = Mn and Fe, respectively. Hybridization of the e_g M 3d and O 2p orbitals partially delocalizes the charge over the oxygen atoms. Sr doping enhances this effect,[39] which further affects $\Delta E_{f,vac}$. In fact, we find that $\Delta E_{f,vac}(x_{Sr})$ directly (inversely) correlates with the percentage of extra charge that delocalizes onto the oxygen sublattice (Figure 5, bottom). This percentage is still low for Mn (∼40−50%) because a partial local reduction of Mn cations is retained for both x_{Sr} = 0.25 and 0.5.[31] Surprisingly, almost no local reduction occurs for Fe ions in LSF; the charge left by the oxygen vacancy formation is mostly accommodated by the oxygen sublattice (∼80%). The very low $\Delta E_{f,vac}$ for LSF are therefore due to favorable delocalization of this charge onto oxygen atoms, thus minimizing repulsion due to the defect. In general, larger amounts of extra charge deposited onto oxygen correspond to lower vacancy formation energies. As shown below, we find that $\Delta E_{f,vac}$ in SFMO-based materials also feature this behavior.

dx.doi.org/10.1021/ar4003174 | Acc. Chem. Res. 2014, 47, 3340−3348

3.3. $Sr_2Fe_{2-x}Mo_xO_{6-\delta}$ (x = 1.0, 0.5)

Antisite defects, naturally present in $SFMO_{1.0}$ perovskites, allow us to analyze oxygen vacancy formation within different local environments, that is, those occurring along Fe−O−Mo, Fe−O−Fe, and Mo−O−Mo bonds.[26] The average $\Delta E_{f,vac}$ of these three types of oxygen vacancies are shown in Figure 6 (left).

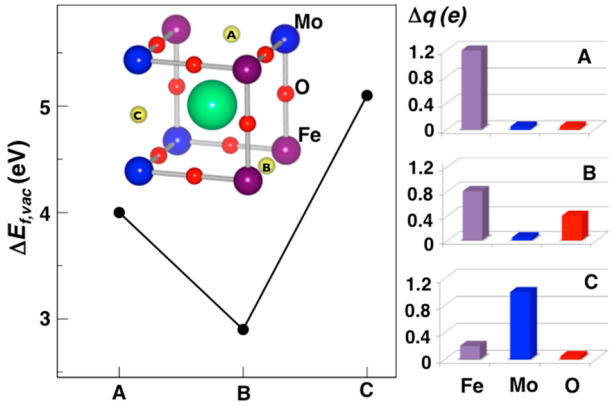

Figure 6. (left) Oxygen vacancy formation energies, $\Delta E_{f,vac}$, along A (Fe−O−Mo), B (Fe−O−Fe), and C (Mo−O−Mo) bonds in $SFMO_{1.0}$. $V_O^{\bullet\bullet}$ shown in yellow. Adapted from ref 26. (right) Corresponding distribution among the Fe, Mo, and O sublattices of the extra charge left behind upon oxygen vacancy formation.

The 3−5 eV range in energy is similar to that for AMO_3 materials. However, $\Delta E_{f,vac}$ along the Fe−O−Fe bonds are significantly lower than those along Fe−O−Mo and Mo−O−Mo bonds by ∼1 and 2 eV, respectively. As in the AMO_3 series, the trend $\Delta E_{f,vac}$(Fe−$V_O^{\bullet\bullet}$−Fe) < $\Delta E_{f,vac}$(Fe−$V_O^{\bullet\bullet}$−Mo) < $\Delta E_{f,vac}$(Mo−$V_O^{\bullet\bullet}$−Mo) follows the bond strength rule, since Fe is a late TM and Mo is an early TM. Moreover, analyzing electron density differences upon oxygen vacancy formation shows that most of the extra charge remains localized on Mo sites in the Mo−$V_O^{\bullet\bullet}$−Mo case, whereas Fe and O sublattices share the extra charge in the Fe−$V_O^{\bullet\bullet}$−Fe (Figure 6, right). Thus, excess Fe (instead of Mo) should provide SFMO-based materials with higher concentrations of oxygen vacancies that facilitate oxide ion diffusion.

Indeed, the Fe-rich $SFMO_{0.5}$ performs extremely efficiently in symmetric IT-SOFCs. Its ionic conductivity rivals that of Co-containing cathodes such as $La_{0.6}Sr_{0.4}CoO_3$ and $La_{0.6}Sr_{0.4}Fe_{0.8}Co_{0.2}O_3$. In joint experimental and theoretical work,[27] we explained why the $SFMO_{0.5}$ structure yields excellent MIEC properties. First, $SFMO_{0.5}$ is a nonstoichiometric solid. Powder neutron diffraction data determined an oxygen-deficient composition of $Sr_2Fe_{1.5}Mo_{0.5}O_{6-\delta}$ (δ_{exp} = 0.10(2)). No Fe/Mo ordering is found, in agreement with the theoretically predicted lower energy of the cell without Mo aggregation, that is, that with Mo in the two opposite vertices of the cube formed by TM ions (Figure 7, inset). Moreover, oxygen vacancies can arise from two possible types, those from Fe−O−Fe bonds or from Fe−O−Mo bonds (no Mo−O−Mo are expected in $SFMO_{0.5}$ with homogeneously distributed Fe/Mo, and as Figure 6 shows, these are the least favorable). Figure 7 (top) shows calculated $\Delta E_{f,vac}$(Fe−$V_O^{\bullet\bullet}$−Fe) and $\Delta E_{f,vac}$(Fe−$V_O^{\bullet\bullet}$−Mo) in $SFMO_{0.5}$ for different concentrations of oxygen vacancies (δ_{theo} = 0.25, 0.125, and 0.0625). $\Delta E_{f,vac}$(Fe−$V_O^{\bullet\bullet}$−Fe) appears to be *nearly zero* for $\delta_{theo} \approx \delta_{exp}$, confirming $SFMO_{0.5}$'s nonstoichiometry. As expected, $\Delta E_{f,vac}$(Fe−$V_O^{\bullet\bullet}$−Fe) is much lower

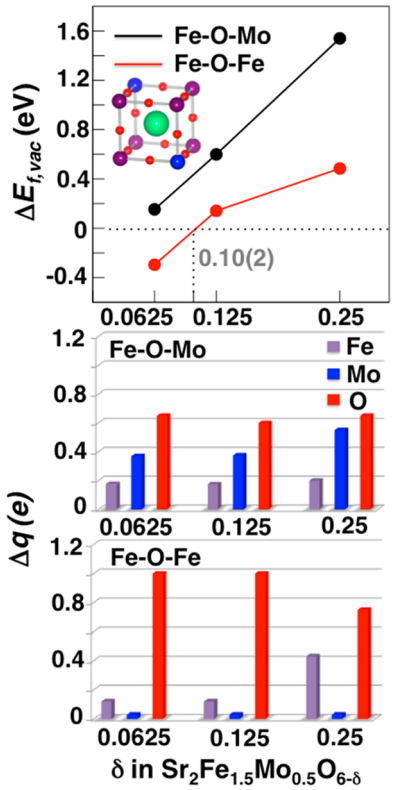

Figure 7. (top) Oxygen vacancy formation energies, $\Delta E_{f,vac}$, as a function of oxygen vacancy concentration δ along Fe−O−Mo and Fe−O−Fe bonds in $SFMO_{0.5}$. Color code as in Figure 6. Experimental δ = 0.10(2) indicated [ref 27]. (middle and bottom) Corresponding distribution of the extra charge remaining within the Fe, Mo, and O sublattices upon oxygen vacancy formation.

than $\Delta E_{f,vac}$(Fe−$V_O^{\bullet\bullet}$−Mo) at all δ, explaining the observed selectivity in oxygen sites exhibiting vacancies. As was found in $La_{1-x}Sr_xFeO_3$, the facile electron delocalization onto the oxygen sublattice upon reduction causes the extraordinarily low $\Delta E_{f,vac}$(Fe−$V_O^{\bullet\bullet}$−Fe) (Figure 7, bottom). The resulting inherent oxygen vacancy concentration likely boosts oxygen mobility, since the diffusion process will thus depend on only the migration barrier.

4. DIFFUSION COEFFICIENTS

DFT+U accurately predicts energetic, structural, and electronic properties of many strongly correlated materials at different temperatures. Calculation of kinetic coefficients, such as diffusivity, can be more challenging. The self-diffusion coefficient, D_O, for a vacancy-mediated hopping mechanism can be expressed in terms of the vacancy diffusion coefficient, D_v, within transition state theory[30,32,41,42] as

$$D_O = \frac{C_v}{C_O} D_v = \frac{C_v}{3 - C_v} D_v \approx \left(\frac{1}{\sqrt{p_{O_2}}} e^{\Delta S_{f,vac}/k_B} e^{-\Delta H_{f,vac}/(k_B T)} \right) \times \left(\frac{1}{6} \nu_0 a^2 e^{\Delta S^{\ddagger}/k_B} e^{-\Delta H_{migr}/(k_B T)} \right) \quad (5)$$

where C_O and C_v are the oxygen and oxygen vacancy concentrations, respectively, expressed in moles per mole of ABO_3 and we consider dilute vacancies. The apparent activation energy for diffusion is the sum of the enthalpies of formation and migration of an oxygen vacancy. The temperature-dependent entropic contributions account for the entropy change upon

dx.doi.org/10.1021/ar4003174 | Acc. Chem. Res. 2014, 47, 3340−3348

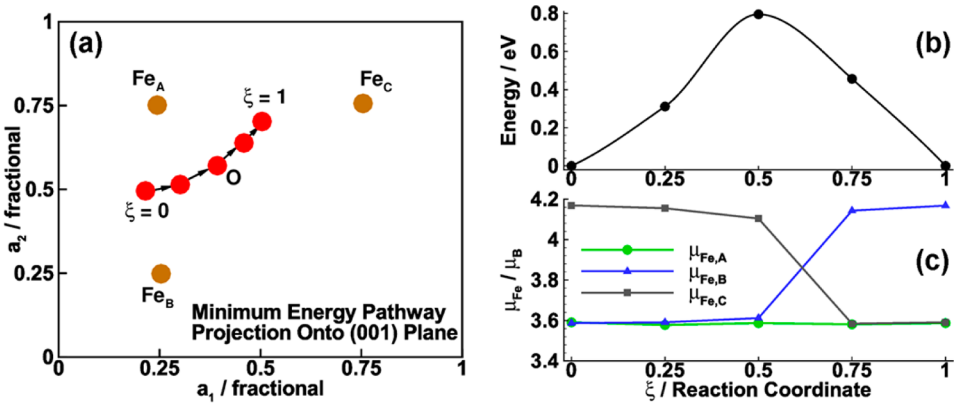

Figure 8. (a) Minimum energy path, (b) energy profile, and (c) magnetic moment profile for oxide ion migration in $LaFeO_3$. Reprinted with permission from ref 29. Copyright 2013 American Chemical Society.

defect formation and the thermal expansion effects at high SOFC operating temperatures.[29,41] D_O is related to the tracer diffusion coefficient, D_O^*, through the correlation factor, f ($f \approx 0.69$ for perovskites[43]), and to the chemical diffusion coefficient, D_{chem}, through the thermodynamic factor, γ. Calculating ΔH_{migr}, ν_0, and $\Delta S^{\ddagger}$ requires knowledge of the transition state (TS) structure. We identify the minimum energy path and its TS using the climbing image nudged elastic band method.[44] We include vibrational entropic effects via calculation of the real phonon frequencies (ν_i) of the initial minimum state and the TS, obtained at the Γ point from the eigenvalues of the Hessian matrix. We neglect configurational entropy terms because of the low concentration of vacancies in our materials.

For the prototypical $LaMO_3$ series, experiments indicate that O^{2-} migration energies are very similar (~0.8−0.9 eV) and not strongly dependent on Sr-doping.[45] We chose $LaFeO_3$ as a representative case to study O^{2-} migration in $La_{1-x}Sr_xMO_3$. Our calculations confirm the curved two-dimensional pathway, a well-known feature in perovskite-type materials.[46] The migrating oxide ion moves in a plane that contains four TM ions (Fe in this case) framed by two La atoms above and below its center (Figure 8, left). Our predicted migration barrier, ΔH_{migr} = 0.79 eV, matches the value from oxygen tracer experiments (ΔH_{migr} =0.77 eV).[43] Localized reduction adjacent to the vacant site couples electron transfer with ion motion, as shown by the abrupt change in Fe magnetic moments during the oxide ion migration (Figure 8, right). We cannot expect analogous coupled electron transfer for $La_{1-x}Sr_xMO_3$ ($x_{Sr} > 0$) materials with delocalized extra charge. However, this electronic feature should have little effect on the migration barrier, which we have shown to be largely governed by steric and electrostatic effects.[29]

Calculating diffusion coefficients that are directly comparable with experiment requires accounting for oxygen vacancy concentrations (C_v in eq 5). An artificially high $\Delta E_{f,vac}$ will lead to artificially low C_vs in perfect $LaFeO_3$, resulting in diffusion coefficients D_O several orders of magnitude in error. We recently showed that accounting for the slight La sub-stoichiometry observed in experiments with $LaFeO_3$ corrects these discrepancies.[30] We found that even a small concentration of La vacancies, V'''_{La}, lead to dramatically higher oxygen vacancy concentrations. V'''_{La} introduces holes that compensate the extra charge from a $V_O^{\bullet\bullet}$, just as Sr did in previous examples. *Thus, promoting cation vacancies is a route to increasing oxygen vacancy concentrations.*

Besides being nonstoichiometric, $SFMO_{0.5}$ also exhibits unusual migration features compared with $LaMO_3$. Preferred oxygen vacancies in $SFMO_{0.5}$ are those along Fe−O−Fe bonds (*vide supra*), so we considered the migration pathway from a Fe−O−Fe occupied site to the nearest Fe−$V_O^{\bullet\bullet}$−Fe. As with other perovskites, oxide ion migration follows a curved path in a four-atom plane. This plane contains three iron atoms (involved in the migration) and a Mo atom at the opposite, fourth corner. The calculated migration energy for this jump (Figure 9, A → B) is ~0.3 eV, much lower than typical values

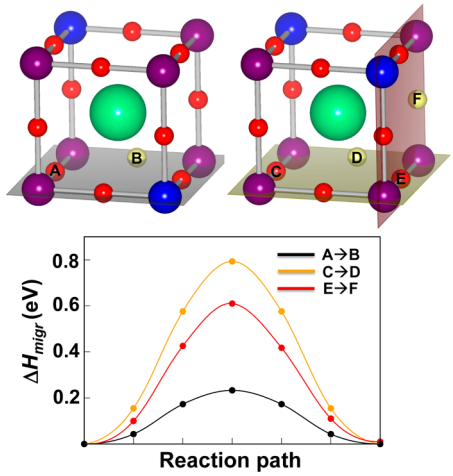

Figure 9. (top) Diffusion planes showing three different (A → B, C → D, and E → F) Fe−O−Fe → Fe−$V_O^{\bullet\bullet}$−Fe jumps in $SFMO_{0.5}$. Color code as in Figure 6. (bottom) Corresponding energy profiles. Adapted from ref 28.

(~0.8−0.9 eV) measured and calculated for La,Sr-based perovskites. The calculated self-diffusion coefficient (at 750 °C) with this migration barrier (taking $\Delta H_{f,vac}$ = 0 due to SFMO's nonstoichiometry) is 5.1 × 10^{-6} cm^2 s^{-1}.[28] Although this is very close to the D_{chem} reported by Chen and co-workers (5.0 × 10^{-6} cm^2 s^{-1}),[47] the γ factor mentioned above brings uncertainty of approximately two orders of magnitude.

Interestingly, the migration barrier for the parent material without Mo, namely, $SrFeO_3$, is ~0.9 eV.[48] Thus, Mo plays an important role in oxygen diffusion. We analyzed this role by computing the migration barrier heights also for Fe−O−Fe → Fe−$V_O^{\bullet\bullet}$−Fe jumps in a layered cell with varying Mo configurations. Having no Mo cation in the migration plane (Figure 9, C → D) increases the migration energy by 0.4 eV, and having a layered Mo distribution (Figure 9, E → F) increases it further by 0.2 eV

dx.doi.org/10.1021/ar4003174 | Acc. Chem. Res. 2014, 47, 3340−3348

(Figure 9, bottom). We observed no change in atomic Bader charges, magnetic moments, or PDOS along the migration pathway in any of the three jumps described above. The similar Shannon ionic radii[49] of Fe(III) and Fe(IV) in 6-fold coordination (0.64 and 0.58 Å, respectively) and that of Mo(VI) (0.59 Å) rule out steric effects determining the diffusion behavior. Thus, we conclude that the differences in migration barriers arise only from Mo-based electrostatic effects. These results suggest that attraction between the highly charged $Mo^{5+\delta}$ cation and the negatively charged oxygen ion produces a lower migration energy when the Mo's are closer to the migration path. Furthermore, we find that the Madelung potential of the crystal stabilizes the TS more for the homogeneous Fe/Mo case than for the layered one.[28]

5. CONCLUSIONS

This Account details the successful application of the DFT+U method with *ab initio*-derived $U-J$ values to explain oxide ion diffusion in two classes of cathode materials for SOFC applications: $La_{1-x}Sr_xM_xO_3$ and $Sr_2Fe_{2-x}Mo_xO_6$. QM calculations elucidated the microscopic effects governing the two processes that determine diffusivity in these materials, that is, oxygen vacancy formation and oxygen migration. We then showed how the oxide ion diffusion coefficients measured in experiments can be accurately predicted from first-principles methods. Our insights clarify several points:

- In $LaMO_3$ materials, the availability of vacant oxygen sites that allow oxide ion transport governs oxide ion diffusion. Thus, the oxygen vacancy formation energy, $\Delta E_{f,vac}$, is a critical descriptor for this process. The electronic rearrangement upon oxygen vacancy formation involves breaking two TM−oxygen bonds and reducing two TMs closest to the vacancy. Weaker M−O bonds and M^{3+} ions with greater electron affinities facilitate oxygen vacancy formation.
- In Sr-doped $LaMO_3$ materials, aliovalent substitution at the La site forms holes that affect electronic states at the valence band edge and consequently the defect chemistry. These holes facilitate the reduction produced by the electrons left behind when the oxygen vacancy forms, via charge compensation. The p-type character also increases the hybridization of the e_g transition metal 3d and oxygen 2p states, allowing delocalization of the extra charge across the M−O sublattice. These two factors significantly lower oxygen vacancy formation energies of $La_{1-x}Sr_xM_xO_3$ compared to $LaMO_3$.
- For $LaFeO_3$-based materials, calculated migration barriers (∼0.8 eV) are in excellent agreement with experiments. By accounting for La vacancies, a quantitative match with the experimental D_O is achieved. As found with Sr-doping, A-site vacancies introduce holes in the system lowering $\Delta E_{f,vac}$ and consequently increasing the concentration of vacant sites on oxygen sublattice. Cation vacancies indirectly promote oxide ion diffusion.
- In $Sr_2Fe_{2-x}Mo_xO_6$ materials, the electronic features and oxide ion diffusion largely depend on the Fe:Mo ratio. Fe-rich compositions exhibit lower oxygen vacancy formation energies and better oxide ion transport properties, because Mo−O bonds are stronger and electron density is more localized at Mo centers upon reduction.
- Theory and experiment both find that $Sr_2Fe_{1.5}Mo_{0.5}O_{6-\delta}$ is inherently nonstoichiometric. Migration barrier heights govern oxide ion diffusion in this material. Even though highly charged Mo^{6+} centers hinder oxygen vacancy formation, they stabilize TS structures and lower the migration barrier to ∼0.3 eV. Our predicted oxide ion diffusion coefficient is very high and agrees with recent experimental estimates.

In summary, $\Delta E_{f,vac}$ is a robust descriptor for evaluating the oxide ion transport properties of perovskite oxides used as SOFC cathodes. There is also a direct relationship between the $\Delta E_{f,vac}$ values and (i) the transition metal−oxygen bond strength and (ii) the degree to which the O sublattice accommodates the vacancy's extra charge. We derived QM-inspired design principles for improved IT-SOFC cathodes: (1) mid-to-late transition metal ions with weak M−O bonds and high electron affinities should be incorporated, (2) dopants and defect engineering should exploit hybridization of M 3d and O 2p states to enhance charge delocalization, and (3) the Fe:Mo ratio in SFMO-based materials should be optimized to include more iron to enhance oxygen nonstoichiometry. Further studies on ORR electrocatalysis and oxygen surface exchange rates are ongoing.

AUTHOR INFORMATION

Funding

This work was supported as part of HeteroFoaM, an Energy Frontier Research Center funded by the U.S. Department of Energy, Office of Science, Office of Basic Energy Sciences under Award Number DE-SC0001061.

Notes

The authors declare no competing financial interest.

Biographies

Ana B. Muñoz-García graduated (*Valedictorian*) in Chemistry in 2006 and obtained her Ph.D. in Theoretical Chemistry and Computational Modeling in 2011 from the Universidad Autónoma de Madrid. After one year as a Postdoctoral Research Associate at Princeton University, she became an Assistant Professor at the Università di Napoli Federico II.

Andrew M. Ritzmann obtained a B.S. in Chemical Engineering (*magna cum laude*) from Cornell University in 2005. Since 2008, he has been a graduate student at Princeton University.

Michele Pavone graduated (*cum laude*) in Chemistry and obtained his Ph.D. in Chemical Sciences from the Università di Napoli Federico II where he is now an Assistant Professor. From 2010 to 2012, he was a Postdoctoral Research Associate at Princeton University.

John A. Keith obtained his B.A. with high honors in chemistry from Wesleyan University and his Ph.D. in chemistry from Caltech. After an Alexander von Humboldt postdoctoral fellowship at the University of Ulm, he was an Associate Research Scholar in the Carter group at Princeton. In 2013, he became the inaugural R.K. Mellon Faculty Fellow in Energy at the University of Pittsburgh.

Emily A. Carter is the Founding Director of the Andlinger Center for Energy and the Environment at Princeton University and the Gerhard R. Andlinger Professor in Energy and the Environment, as well as Professor of Mechanical and Aerospace Engineering and Applied and Computational Mathematics.

REFERENCES

(1) Boudghene-Stambouli, A.; Traversa, E. Solid oxide fuel Cells (SOFCs): A Review of an Environmentally Clean and Efficient Source of Energy. *Renewable Sustainable Energy Rev.* **2002**, *6*, 433−455.
(2) Adler, S. B. Factors Governing Oxygen Reduction in Solid Oxide Fuel Cell Cathodes. *Chem. Rev.* **2004**, *104*, 4791−4843.
(3) Chroneos, A.; Yildiz, B.; Tarancón, A.; Parfitt, D.; Kilner, J. A. Oxygen Diffusion in Solid Oxide Fuel Cell Cathode and Electrolyte

Materials: Mechanistic Insights from Atomistic Simulations. *Energy Environ. Sci.* **2011**, *4*, 2774−2789.
(4) Yueh-Lin, L.; Kleis, J.; Rossmeisl, J.; Shao-Horn, Y.; Morgan, D. Prediction of Solid Oxide Fuel Cell Cathode Activity with First-Principles Descriptors. *Energy Environ. Sci.* **2011**, *4*, 3966−3970.
(5) Kuklja, M. M.; Kotomin, E. A.; Merkle, R.; Mastrikov, Y. A.; Maier, J. Combined Theoretical and Experimental Analysis of Processes Determining Cathode Performance in Solid Oxide Fuel Cells. *Phys. Chem. Chem. Phys.* **2013**, *15*, 5443−5471.
(6) Kohn, W.; Sham, L. J. Self-Consistent Equations Including Exchange and Correlation Effects. *Phys. Rev.* **1965**, *140*, A1133−A1138.
(7) Wachsman, E. D.; Singhal, S. C. Solid Oxide Fuel Cell Commercialization, Research, and Challenges. *Am. Ceram. Soc. Bull.* **2010**, *89*, 22−32.
(8) Liu, Q.; Dong, X.; Xiao, G.; Ma, S.; Zhao, F.; Chen, F. A Novel Electrode Material for Symmetrical SOFCs. *Adv. Mater.* **2010**, *22*, 5478−5482.
(9) Carter, E. A. Challenges in Modeling Materials Properties without Experimental Input. *Science* **2008**, *321*, 800−803.
(10) Huang, P.; Carter, E. A. Advances in Correlated Electronic Structure Methods for Solids, Surfaces, and Nanostructures. *Annu. Rev. Phys. Chem.* **2008**, *59*, 261−290.
(11) Anisimov, V. I.; Zaanen, J.; Andersen, O. K. Band Theory and Mott Insulators: Hubbard *U* Instead of Stoner *I*. *Phys. Rev. B* **1991**, *44*, 943−954.
(12) Becke, A. D. A New Mixing of Hartree-Fock and Local Density-Functional Theories. *J. Chem. Phys.* **1993**, *98*, 1372−1377.
(13) Perdew, J. P.; Burke, K.; Ernzerhof, M. Generalized Gradient Approximation Made Simple. *Phys. Rev. Lett.* **1996**, *77*, 3865−3868.
(14) Johnson, B. G.; Gill, P. M. W.; Pople, J. A. The Performance of a Family of Density Functional Methods. *J. Chem. Phys.* **1993**, *98*, 5612−5626.
(15) Mosey, N. J.; Carter, E. A. Ab initio Evaluation of Coulomb and Exchange Parameters for DFT+U Calculations. *Phys. Rev. B* **2007**, *76*, No. 155123.
(16) Mosey, N. J.; Liao, P.; Carter, E. A. Rotationally Invariant *Ab Initio* Evaluation of Coulomb and Exchange Parameters for DFT+*U* Calculations. *J. Chem. Phys.* **2008**, *129*, No. 014103.
(17) Kulik, H. J.; Cococcioni, M.; Scherlis, D. A.; Marzari, N. Density Functional Theory in Transition-Metal Chemistry: A Self-Consistent Hubbard U Approach. *Phys. Rev. Lett.* **2006**, *97*, No. 103001.
(18) Toroker, M. C.; Kanan, D. K.; Alidoust, N.; Isseroff, L. Y.; Liao, P.; Carter, E. A. First Principles Scheme to Evaluate Band Edge Positions in Potential Transition Metal Oxide Photocatalysts and Photoelectrodes. *Phys. Chem. Chem. Phys.* **2011**, *13*, 16644−16654.
(19) Kanan, D. K.; Carter, E. A. Band Gap Engineering of MnO via ZnO Alloying: A Potential New Visible-Light Photocatalyst. *J. Phys. Chem. C* **2012**, *116*, 9876−9887.
(20) Yu, K.; Carter, E. A. Communication: Comparing *ab Initio* Methods of Obtaining Effective U Parameters for Closed-Shell Materials. *J. Chem. Phys.* **2014**, *140*, No. 121105.
(21) Hashimoto, T.; Ishibashi, S.; Terakura, K. Jahn-Teller Distortion and Magnetic Structure in $LaMnO_3$: A First-principles Theoretical Study with Full Structure Optimizations. *Phys. Rev. B* **2010**, *82*, No. 045124.
(22) Kobayashi, K. I.; Kimura, T.; Sawada, H.; Terakura, K.; Tokura, Y. Room-Temperature Magnetoresistance in an Oxide Material with an Ordered Double-Perovskite Structure. *Nature* **1998**, *395*, 677−680.
(23) Kröger, F. A.; Vink, H. J. Relations between the Concentrations of Imperfections in Crystalline Solids. *Solid State Phys.* **1956**, *3*, 307−435.
(24) Kresse, G.; Furthmüller, J. Efficient Iterative Schemes for *Ab Initio* Total-Energy Calculations Using a Plane-Wave Basis Set. *Phys. Rev. B* **1996**, *54*, 11169−11186.
(25) Pavone, M.; Ritzmann, A. M.; Carter, E. A. Quantum-Mechanics-Based Design Principles for Solid Oxide Fuel Cell Cathode Materials. *Energy Environ. Sci.* **2011**, *4*, 4933−4937.
(26) Muñoz-García, A. B.; Pavone, M.; Carter, E. A. Effect of Antisite Defects on the Formation of Oxygen Vacancies in Sr_2FeMoO_6: Implications for Ion and Electron Transport. *Chem. Mater.* **2011**, *23*, 4525−4536.
(27) Muñoz-García, A. B.; Bugaris, D. E.; Pavone, M.; Hodges, J. P.; Huq, A.; Chen, F.; zur Loye, H.-C.; Carter, E. A. Unveiling Structure-Property Relationships in $Sr_2Fe_{1.5}M_{0.5}O_{6-\delta}$, an Electrode Material for Symmetric Solid Oxide Fuel Cells. *J. Am. Chem. Soc.* **2012**, *134*, 6826−6833.
(28) Muñoz-García, A. B.; Pavone, M.; Ritzmann, A. M.; Carter, E. A. Oxide Ion Transport in $Sr_2Fe_{1.5}M_{0.5}O_{6-\delta}$, a Mixed Ion-Electron Conductor: New Insights from First-Principles Modeling. *Phys. Chem. Chem. Phys.* **2013**, *15*, 6250−6259.
(29) Ritzmann, A. M.; Muñoz-García, A. B.; Pavone, M.; Keith, J. A.; Carter, E. A. *Ab Initio* DFT+U Analysis of Oxygen Vacancy Formation and Migration in $La_{1-x}Sr_xFeO_{3-\delta}$ (x = 0, 0.25, 0.50). *Chem. Mater.* **2013**, *25*, 3011−3019.
(30) Ritzmann, A. M.; Muñoz-García, A. B.; Pavone, M.; Keith, J. A.; Carter, E. A. *Ab Initio* Evaluation of Oxygen Diffusivity in $LaFeO_3$: The Role of La Vacancies. *MRS Commun.* **2013**, *3*, 161−166.
(31) Pavone, M.; Muñoz-García, A. B.; Ritzmann, A. M.; Carter, E. A. *Ab Initio* Study of Lanthanum Strontium Manganite: Insights into Electronic Features and Oxygen Vacancy Formation. *J. Phys. Chem. C* **2014**, DOI: 10.1021/jp500352h.
(32) Ritzmann, A. M.; Pavone, M.; Muñoz-García, A. B.; Keith, J. A.; Carter, E. A. *Ab Initio* DFT+U Analysis of Oxygen Transport in $LaCoO_3$: The Effect of Co^{3+} Spin States. *J. Mater. Chem. A* **2014**, *2*, 8060−8074.
(33) Jiang, S. P.; Li, J. In *Solid Oxide Fuel Cells: Materials Properties and Performances*; Fergus, J.W., Hui, R., Li, X., Wilkinson, D.P., Zhang, J., Eds.; CRC Press 2009; pp 131−137.
(34) Tang, W.; Sanville, E.; Henkelman, G. A Grid-based Bader Analysis Algorithm without Lattice Bias. *J. Phys.: Condens. Matter* **2009**, *21*, No. 084204.
(35) Carter, E. A.; Goddard, W. A., III Early- versus Late-Transition-Metal-Oxo Bonds: The Electronic Structure of Oxovanadium(1+) and Oxoruthenium(1+). *J. Phys. Chem.* **1988**, *92*, 2109−2115.
(36) Winkler, J. R.; Gray, H. B. Electronic Structures of Oxo-Metal Ions. In *Molecular Electronic Structures of Transition Metal Complexes I*; Mingos, D. M. P., Day, P., Dahl, J. P., Eds.; Structure and Bonding; Springer: Berlin/Heidelberg, 2012; pp 17−28.
(37) Radaelli, P. G.; Cheong, S.-W. Structural Phenomena Associated with the Spin-state Transition in $LaCoO_3$. *Phys. Rev. B* **2002**, *66*, No. 094408.
(38) Hong, W. T.; Gadre, M.; Lee, Y.-L.; Biegalski, M. D.; Christen, H. M.; Morgan, D.; Shao-Horn, Y. Tuning the Spin State in $LaCoO_3$ Thin Films for Enhanced High-Temperature Oxygen Electrocatalysis. *J. Phys. Chem. Lett.* **2013**, *4*, 2493−2499.
(39) Kilner, J. A.; Berenov, A.; Rossiny, J. In *Perovskite Oxide for Solid Oxide Fuel Cells*; Ishihara, T., Ed.; Springer: Dordrecht, the Netherlands, 2009; pp 95−116.
(40) Mizusaki, J.; Sasamoto, T.; Cannon, W. R.; Bowen, H. K. Electronic Conductivity, Seebeck Coefficient, and Defect Structure of $La_{1-x}Sr_xFeO_3$ (x = 0.l, 0.25). *J. Am. Ceram. Soc.* **1983**, *66*, 247−252.
(41) Vineyard, G. H. Frequency Factors and Isotope Effects in Solid-State Rate Processes. *J. Phys. Chem. Solids* **1957**, *3*, 121−127.
(42) Marino, K. A.; Carter, E. A. First-principles Characterization of Ni Diffusion Kinetics in β-NiAl. *Phys. Rev. B* **2008**, *78*, No. 184105.
(43) Ishigaki, T.; Yamauchi, S.; Kishio, K.; Mizusaki, J.; Fueki, K. Diffusion of Oxide Ions in Perovskite-type Oxides. *J. Solid State Chem.* **1988**, *73*, 179−187.
(44) Henkelman, G.; Uberuaga, B. P.; Jónsson, H. A Climbing Image Nudged Elastic Band Method for Finding Saddle Points and Minimum Energy Paths. *J. Chem. Phys.* **2000**, *113*, 9901−9904.
(45) Mastrikov, Y. A.; Merkle, R.; Kotomin, E. A.; Kuklja, M. M.; Maier, J. Formation and Migration of Oxygen Vacancies in $La_{1-x}Sr_xCo_{1-y}Fe_yO_{3-\delta}$ Perovskites: Insight from ab Initio Calculations and Comparison with $Ba_{1-x}Sr_xCo_{1-y}Fe_yO_{3-\delta}$. *Phys. Chem. Chem. Phys.* **2013**, *15*, 911−918.

(46) Islam, M. S. Ionic Transport in ABO_3 Perovskite Oxides: A Computer Modeling Tour. *J. Mater. Chem.* **2000**, *10*, 1027−1038.
(47) Xiao, G.; Liu, Q.; Zhao, F.; Zhang, L.; Xia, C.; Chen, F. $Sr_2Fe_{1.5}Mo_{0.5}O_6$ as Cathodes for Intermediate-Temperature Solid Oxide Fuel Cells with $La_{0.8}Sr_{0.2}Ga_{0.87}Mg_{0.13}O_3$ Electrolyte. *J. Electrochem. Soc.* **2011**, *158*, B455−B460.
(48) Wang, L.; Merkle, R.; Maier, J. Surface Kinetics and Mechanism of Oxygen Incorporation into $Ba_{1-x}Sr_xCo_yFe_{1-y}O_{3-\delta}$ SOFC Microelectrodes. *J. Electrochem. Soc.* **2010**, *157*, B1802−B1808.
(49) Shannon, R. D. Revised Effective Ionic Radii and Systematic Studies of Interatomic Distances in Halides and Chalcogenides. *Acta Crystallogr.* **1976**, *A32*, 751−767.